Editors' Suggestion

Shear-Driven Solidification and Nonlinear Elasticity in Epithelial Tissues

Junxiang Huang,[1] James O. Cochran,[2] Suzanne M. Fielding,[2] M. Cristina Marchetti,[3] and Dapeng Bi[1]
[1]Department of Physics, Northeastern University, Boston, Massachusetts 02115, USA
[2]Department of Physics, Durham University, Science Laboratories, South Road, Durham DH1 3LE, United Kingdom
[3]Department of Physics, University of California, Santa Barbara, California 93106, USA

(Received 29 September 2021; accepted 31 March 2022; published 27 April 2022)

Biological processes, from morphogenesis to tumor invasion, spontaneously generate shear stresses inside living tissue. The mechanisms that govern the transmission of mechanical forces in epithelia and the collective response of the tissue to bulk shear deformations remain, however, poorly understood. Using a minimal cell-based computational model, we investigate the constitutive relation of confluent tissues under simple shear deformation. We show that an initially undeformed fluidlike tissue acquires finite rigidity above a critical applied strain. This is akin to the shear-driven rigidity observed in other soft matter systems. Interestingly, shear-driven rigidity can be understood by a critical scaling analysis in the vicinity of the second order critical point that governs the liquid-solid transition of the undeformed system. We further show that a solidlike tissue responds linearly only to small strains and but then switches to a nonlinear response at larger stains, with substantial stiffening. Finally, we propose a mean-field formulation for cells under shear that offers a simple physical explanation of shear-driven rigidity and nonlinear response in a tissue.

DOI: 10.1103/PhysRevLett.128.178001

Monolayers of tightly connected cells provide essential physical barriers and filters to all organs *in vivo*. The tight connections between cells allow the tissue to resist external deformation and withstand stress, while maintaining its integrity. At the single cell level, researchers have used a broad repertoire of experimental techniques [1–6] to reveal a rich mechanical behavior, including power-law rheology [7] and stress stiffening [8]. At the mesoscopic level, traction force microscopy has allowed the mapping of intercellular forces [9–11], revealing a rough stress landscape, with spatial fluctuations correlated over several cells [12–15].

There is increasing consensus that mechanical deformations can directly influence collective cell behavior [16–20] and play a central role in driving developmental processes [21–28], physiology [14,29–33], and tumor progression [34–36]. Experiments [30,37–39] have shown that epithelial monolayers respond nonlinearly to external mechanical stretch, with observed stress stiffening and even fracturing. Similar behavior has been observed in tissues deformed by internal active motile forces [40] and in curved epithelial sheets enclosing an expanding lumen [41]. Importantly, these experimental studies have typically focused on probing the behavior of solidlike tissue, where cells do not spontaneously exchange neighbors. On the other hand, the last decade has seen a surge of evidence demonstrating that living tissue can spontaneously undergo transitions between a solidlike (jammed) state and a fluidlike (unjammed) state [42–55]. Despite its fundamental importance and direct relevance to biology, the response of a cell collective to mechanical deformation *at the tissue level* remains poorly understood, especially in the vicinity of the tissue solid-fluid transition.

A growing number of theoretical studies has begun to address this gap. Various groups have used vertex-based models [56,57] to simulate the linear [58] and nonlinear [59–61] rheology of a tissue under steady shear. The effects of active tension fluctuations [60,62] and cell division [63] have been explored. An earlier study [64] has showed that the vertex model exhibits a nonlinear mechanical response qualitatively similar to experiments [37]. Despite this growing body of work, to date there is no systematic study of the mechanical response of an amorphous epithelial tissue near the solid-fluid transition.

Here we use a cell-vertex model to investigate the tissue response to externally imposed shear deformations. We show that a tissue which is fluidlike when undeformed acquires rigidity above a threshold value of the applied strain. This is akin to the shear-driven rigidity of fiber networks and shear jamming in granular matter [65]. The onset of shear-driven rigidity in the liquid state is characterized by a discontinuous jump in the tissue shear modulus, and the size of the jump depends on the distance to the second order liquid-solid critical point of the undeformed system. We find that nonlinear elasticity becomes increasingly dominant closer to the critical point, where the mechanical response is completely nonlinear. This intrinsic critical nonlinearity was also demonstrated in recent work on a vertex models of regular polygons, where it was shown to arise from purely geometric constraints [66]. While Ref. [66] focused on the response to infinitesimal perturbations, demonstrating the failure of linear elasticity, here we examine the nonlinear response in the presence of topological rearrangements that mediate

plasticity. We additionally extend the mean-field (MF) formulation of [66] to account for the emergence of shear-induced rigidity in the liquid state. The MF predicts exactly the nonlinear response and stress-stiffening exponents observed in the simulations.

Model.—We model a 2D cell layer using the Voronoi-based implementation [67,68] of the vertex model [51,57,69–72]. Here, the cell centers $\{\mathbf{r_i}\}$ are the degrees of freedom and their Voronoi tessellation determine the cellular structure [67]. The mechanics of the cell layer is governed by the energy function [73] $E = \sum_{i=1}^{N} [K_A(A_i - A_0)^2 + K_P(P_i - P_0)^2]$. The first term, quadratic in the cell areas $\{A_i\}$, originates from the incompressibility of cell volume, giving rise to a 2D area elasticity constant K_A and preferred area A_0 [57,73]. The second term quadratic in the cell perimeters $\{P_i\}$ arises from the contractility of the cell cortex, with an elastic constant K_P [57]. Here P_0 is the target cell perimeter [74], representing the interfacial tension set by the competition between the cortical tension and the adhesion between adjacent cells [73]. In this Letter, we focus on the case where all cells have homogeneous single cell parameters K_A, K_P, A_0, P_0, while noting that the results are easily generalized to a tissue containing cell-to-cell heterogeneity [69] and are not qualitatively affected by this assumption. We choose $A_0 = \bar{A}$, the mean cell area, which also serves as the length unit. The resulting nondimensionalized energy is

$$E = \sum_{i=1}^{N} \kappa_A(a_i - 1)^2 + (p_i - p_0)^2, \tag{1}$$

with $\kappa_A = K_A\bar{A}/K_P$ the rescaled area elasticity. Here $p_0 = P_0/\sqrt{\bar{A}}$ is a crucial model parameter called target cell shape index. To study tissue response beyond the linear regime [71], we impose quasistatic simple shear using Lees-Edwards boundary conditions [75]. Starting from a strain-free state ($\gamma = 0$), the strain γ is increased in increments of $\Delta\gamma = 2 \times 10^{-3}$, while cell center positions are subject to an affine displacement $\Delta\mathbf{r_i} = \Delta\gamma y_i \hat{\mathbf{x}}$. Following each strain step, Eq. (1) is relaxed using the FIRE algorithm [76] until all forces $\mathbf{F}_i \equiv -\partial E/\partial \mathbf{r_i}$ are vanishingly small ($<10^{-14}$). For all results presented in this Letter, we used 84 random initial configurations and $N = 400$ cells.

The unstrained tissue is known to exhibit a liquid-solid transition as a function of p_0 [71,74,77]. When p_0 is below the critical cell shape index $p_0^* = 3.81$ and $\kappa_A = 0$ the unstrained tissue behaves as a rigid solid, with a finite linear-response shear modulus $G_0 \equiv \lim_{\gamma\to 0} \partial\sigma/\partial\gamma$. When $p_0 \geq p_0^*$, the unstrained tissue is fluid and $G_0 = 0$. This solid-fluid transition at $\gamma = 0$ is now well understood in terms of a Maxwell constraint-counting approach [71,78] and as driven by geometric incompatibility [71,74,79–81].

Nonlinear shear response.—To characterize the mechanical response at finite γ, we compute the tissue shear stress [82–84] $\sigma = \sigma_{xy} \equiv L^{-2} \sum_{i<j} T_{ij}^x l_{ij}^y$, where $\mathbf{l}_{ij}$ is the vector of the junction shared by cells i, j, and L is the simulation box size. At each junction, the line tension vector is given by $\mathbf{T}_{ij} = \partial E/\partial \mathbf{l}_{ij} = 2[(p_i - p_0) + (p_j - p_0)]\hat{l}_{ij}$. The stress-strain relation shown in Fig. 1(a) for a range of values of p_0 and $\kappa_A = 0$ reveals three regimes. For infinitesimal strain the solid responds linearly with modulus G_0. In the fluid, $G_0 = 0$. At intermediate strain ($0 < \gamma < 1$) we observe strong stiffening. In particular, the liquid acquires a finite rigidity for γ above a critical value $\gamma_C(p_0)$. At larger strains ($\gamma \gtrsim 2$), the tissue undergoes plastic rearrangements via T1 transitions, resulting in intermittent stick-slip behavior. We define the dynamic yield stress $\sigma_{\text{yield}}(p_0)$ by averaging σ in the plastic regime ($2 < \gamma < 6$). The yield stress is large in a solid tissue and decreases as p_0 increases, vanishing at $p_0 \sim 4.03$ (see Fig. S1 [85]). The main focus of this Letter is the stress response in the intermediate region of strain stiffening and strain-induced rigidity, which is also the regime most relevant to experiments [37]. We show below that in this regime the linear response ($\gamma \to 0$) cannot predict what happens at finite strain values.

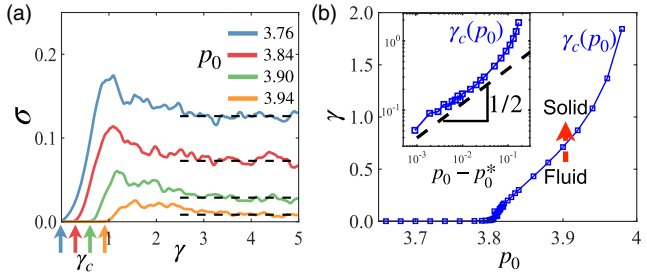

FIG. 1. (a) Stress vs. Strain at different p_0 and $\kappa_A = 0$. An initially fluidlike tissue undergoes strain-driven rigidity above a critical threshold γ_C (location indicated by vertical arrows). (b) The critical strain $\gamma_C(p_0)$ defines a boundary that separates a fluidlike tissue from a solidlike tissue. Inset: γ_c vs p_0 on log-log scale.

Shear-induced rigidity transition.—When the unstrained tissue is fluid ($p_0 > p_0^*$), an applied shear strain $\gamma \geq \gamma_C$ yields a finite stress [Fig. 1(a)]. The line $\gamma_C(p_0)$ where the instantaneous shear modulus $G \equiv \partial\sigma/\partial\gamma$ vanishes identifies a strain-induced rigidity transition [Fig. 1(b)]. In the solid ($p_0 < p_0^*$), we observe stiffening for any finite γ, and $\gamma_C(p_0) = 0$. For $p_0 \in [p_0^*, 4.03]$, a nonzero value of strain is always required for rigidity and $\gamma_C(p_0)$ grows monotonically with p_0. Beyond $p_0 \gtrsim 4$ the tissue remains fluidlike regardless of the applied shear strain. This is consistent with the vanishing of σ_{yield} for $p_0 > 4.03$. The shear stiffening of the liquid was also reported in recent work on a regular (crystalline) vertex model [58], in spring networks [80], and in deformable particle models [93]. The mean-field analysis below provides a universal explanation for this behavior.

The nature of the strain-induced rigidity transition depends on the value of the area stiffness κ_A. This is

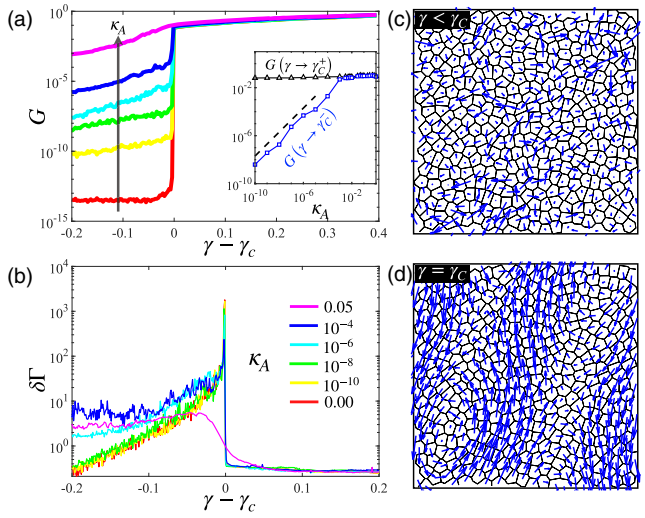

FIG. 2. Strain-driven rigidity transition. (a) The shear modulus G near the onset of the strain-driven solidification for $p_0 = 3.84$ and different area elasticities $\kappa_A = 0, 10^{-10}, 10^{-8}, 10^{-6}, 10^{-4}, 0.05$. Color legends provided in (b). Inset: G immediately below and above the transition shows a gap that narrows with increasing κ_A. The dashed line corresponds to a slope of 1 on a log-log scale. The transition is discontinuous in G at $\gamma = \gamma_C$. (b) The nonaffinity parameter near the onset of the transition for $p_0 = 3.84$ and different κ_A. Nonaffine cell displacements at below (c) and at (d) the onset of the transition.

evident in Fig. 2(a), where we plot G near the rigidity onset as a function of $\gamma - \gamma_C$. At $\kappa_A = 0$, the onset of rigidity is discontinuous. The jump discontinuity at γ_C remains finite well above $\kappa_A = 0$ and becomes vanishingly small and indistinguishable from a continuous increase in G at $\kappa_A \gtrsim 10^{-3}$. For $\gamma < \gamma_C$ the tissue is a marginally rigid solid [79,80] with $G \approx \kappa_A$ [Fig. 2(a), inset]. This is highlighted by the behavior of the fluctuations near the strain-driven rigidity transition, which are quantified with the nonaffinity parameter $\delta\Gamma = (1/N\bar{A}\Delta\gamma^2)\langle(\delta\mathbf{r}_i - \delta\mathbf{r}_i^{\text{affine}})^2\rangle$ [94–96]. Here $\delta\mathbf{r}_i$ is the displacement of cell i after a strain step and $\delta\mathbf{r}_i^{\text{affine}} = \Delta\gamma y_i\hat{\mathbf{x}}$ is the affine deformation of the cell located at $\mathbf{r}_i = (x_i, y_i)$. As shown in Fig. 2(b), at low area elasticity ($\kappa_A \lesssim 10^{-3}$), $\delta\Gamma$ grows monotonically with strain and exhibits a sharp peak at γ_C, which coincides with the rigidity transition. At higher κ_A, there is no pronounced peak in $\delta\Gamma$, indicating a smooth crossover from the marginal solid to a rigid solid, rather than a discontinuous transition.

Relating mechanical response to cell shape.—The strain stiffening behavior above $\gamma_C(p_0)$ can be understood in terms of shear-induced changes in the structural properties of the cellular network. Past work on vertex models has shown that the observed cell shape index, $q \equiv \langle p/\sqrt{a}\rangle$, is an important metric of the rheological state of the tissue [42,51]. We have examined the evolution of this order parameter with applied shear. We note, however, that the applied strain γ does not uniquely define the state of the

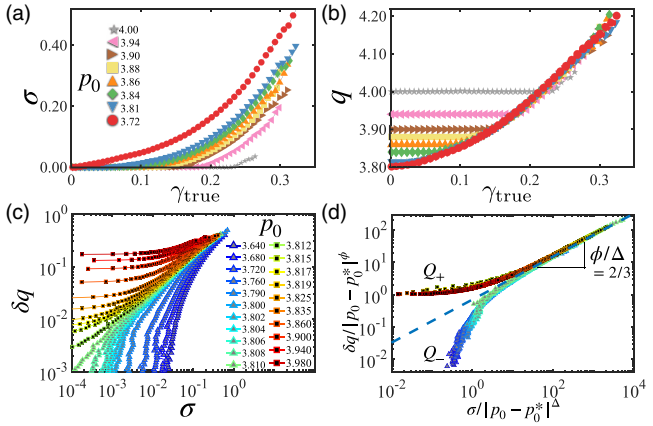

FIG. 3. Cell shapes under shear. (a) A plot of σ as a function of γ_{true} for different p_0's spanning the solid and liquid regimes. (b) The cell shape index q vs the true strain γ_{true} for the same range of p_0 as in (a). (c) A plot of $\delta q \equiv q - p_0^*$ vs σ for various values of p_0 as indicated. (d) Replotting of the data in (c) using the universal scaling ansatz [Eq. (3)]. Here $\Delta = 3/2$, $\phi = 1$. All figures are for $\kappa_A = 0$.

tissue due to plastic events and nonaffine deformations. Instead we use the true strain γ_{true} [97] to quantify the degree of deformation of the tissue. γ_{true} is calculated from the instantaneous deformation tensor of the whole tissue and therefore captures the degree of *cumulative* strain deformation [85]. The motivation for introducing γ_{true} is similar to that behind the fabric tensor in granular materials [98] or the recoverable strain in rheology [99]. In Figs. 3(a) and 3(b) we show the stress σ and the structural order parameter q as functions of γ_{true}. It is evident from Fig. 3(b) that under shear cell shapes in the fluid stay constant at the energetically preferred value p_0 until the fluid strain stiffens, while in the solid q always starts out at the universal value p_0^* and grows quadratically with γ_{true}. This behavior is well described by

$$q = \begin{cases} p_0, & \gamma_{\text{true}} \le \gamma_C(p_0), \\ p_0^* + c\gamma_{\text{true}}^2, & \gamma_{\text{true}} > \gamma_C(p_0). \end{cases} \tag{2}$$

In the next section, we offer a theoretical derivation of this form. A similar functional dependence of the observed cell shape on the cell elongation induced by internally generated active stresses was reported in a recent study of the developing fruit fly [28].

Equation (2) suggests that the quantity $\delta q \equiv q - p_0^*$ can be used as a morphological order parameter, quantifying the deviation of the measured cell shape from the critical cell shape. Moreover, Figs. 3(a) and 3(b) suggest that the three state variables $(\sigma, \gamma_{\text{true}}, \delta q)$ are not independent, and that any two are sufficient to describe the state of the tissue. Therefore, we eliminate γ_{true} and plot δq as a function σ [Fig. 3(c)] for a large range of $p_0 \in [3.72, 4]$. This plot shows typical hallmarks of a critical point, with

qualitatively different behavior above and below p_0^*, suggesting a scaling ansatz

$$\delta q = |p_0 - p_0^*|^{\phi} Q_{\pm}\left(\frac{\sigma}{|p_0 - p_0^*|^{\Delta}}\right). \tag{3}$$

Here $Q_{\pm}(x)$ are the branches of the universal scaling function for $p_0 > p_0^*$ and $p_0 \leq p_0^*$, respectively, with $x = \sigma/|p_0 - p_0^*|^{\Delta}$. This ansatz provides a nearly perfect collapse of the data [Fig. 3(d)], with $\Delta = 3/2$ and $\phi = 1$. For $p_0 > p_0^*$ the behavior is controlled by $Q_+(x)$, with $Q_+(x) \to$ const for $x \to 0$, i.e., $\sigma \to 0$, implying $\delta q \propto |p_0 - p_0^*|^{\phi}$. When $p_0 < p_0^*$, the scaling is controlled by $Q_-(x)$. In the limit of $\delta q \to 0$ (i.e., $y = \delta q/|p_0 - p_0^*|^{\phi} \to 0$), the inverse of Q_- tends to a constant, hence $\sigma \propto |p_0 - p_0^*|^{\Delta}$. For $|p_0 - p_0^*| \to 0$ and $\sigma \gg 0$, the two universal branches merge and $Q_+(x) = Q_-(x) = x^{\phi/\Delta}$.

A nonlinear constitutive equation for sheared tissue.—In tissues strained beyond γ_C both the stress σ [Fig. 1(a)] and the shear modulus G [Fig. 2(a)] are nonlinear functions of the applied strain γ. To quantify the nonlinearity and extract a constitutive equation for the tissue, we use σ, instead of γ, as a state variable and plot G as a function of σ in Fig. 4(a) for various $p_0 \in [3.66, 3.81]$. At small σ, $G = G_0$ is independent of σ, corresponding to linear elasticity. At higher stress, the elastic response is nonlinear and $G \propto (\sigma/\sigma_c)^b$, with $b = 2/3$. Using $G = \partial\sigma/\partial\gamma$ and eliminating G, this yields a constitutive relation $\sigma \propto \gamma^{(1/1-b)} = \gamma^3$. The linear and nonlinear regimes are separated by a critical stress threshold $\sigma_c(p_0) \sim |p_0 - p_0^*|$. The linear-response modulus G_0 also shows power-law scaling in $|p_0 - p_0^*|$ [71,74]. This behavior can be summarized through a scaling ansatz to describe the behavior of G in the vicinity of the critical point p_0^*,

$$G = |p_0 - p_0^*|^{\phi} \mathcal{G}\left(\frac{\sigma}{|p_0 - p_0^*|^{\Delta}}\right). \tag{4}$$

This form provides an excellent collapse of all our data onto a single master curve independent of p_0 [Fig. 4(b)]. From the scaling collapse we obtain $G_0 \propto |p_0 - p_0^*|^{\phi}$ and $\sigma_c \propto |p_0 - p_0^*|^{\Delta}$, where $\Delta = 3/2$ and $\phi = 1$. Crucially, the stress-stiffening scaling collapse [Eq. (4)] is directly related to the cell shape-stress scaling relation [Eq. (3)] as $b = \phi/\Delta$.

Mean-field model of a sheared tissue.—To gain a theoretical understanding of the strain-driven rigidity and emergence of nonlinear elasticity, we examine a mean-field theory (MFT) formulation of the vertex model [66,86,100]. Neglecting cell-cell correlations, we consider the shear deformation of a *single* n-sided polygonal cell. Under affine deformations, the vertex coordinates of a polygon transform according to $\mathbf{R}' = \hat{D}\mathbf{R}$, where $\hat{D}$ is the deformation tensor given by $\hat{D} = \left(\begin{smallmatrix} D_{xx} & D_{xy} \\ D_{yx} & D_{yy} \end{smallmatrix}\right)$. We neglect in Eq. (1) the contribution from cell area which is typically small compared to the perimeter term and examine

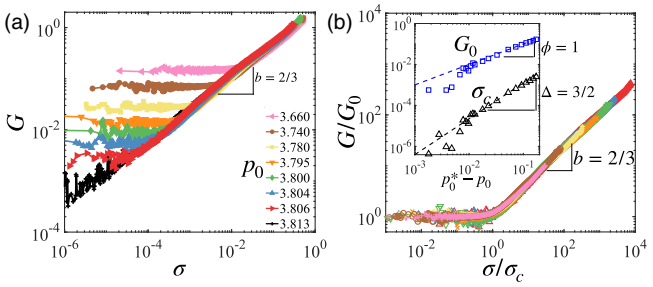

FIG. 4. (a) The shear modulus G vs stress σ at various p_0 and $\kappa_A = 0$. (b) Rescaled G/G_0 vs σ/σ_c for same set of p_0 as in (a).

area-preserving affine deformations with $\det \hat{D} = 1$. For simple shear $D_{yx} = 0$ and $D_{yy} = 1/D_{xx}$, leaving only D_{xx} and D_{xy} as independent components of $\hat{D}$.

The perimeter of a deformed polygon can then be expressed in terms of the components of $\hat{D}$. For example, the perimeter of a quadrilateral ($n = 4$) is given by

$$P = \sqrt{2}\left[\sqrt{D_{xx}^{-2} + (D_{xx} - D_{xy})^2} + \sqrt{D_{xx}^{-2} + (D_{xx} + D_{xy})^2}\right]. \tag{5}$$

Expressions for any deformed n-gon are given in the Supplemental Material [85]. For any n, the isoperimetric inequality defines the perimeters compatible with a fixed area as $P > P_{\text{reg}}$, where P_{reg} is the perimeter of a regular polygon with unit area (e.g., $P_{\text{reg}} = 4$ for $n = 4$). The condition $P(D_{xx}, D_{xy}) \geq P_{\text{reg}}$, with $P(D_{xx}, D_{xy})$ given by Eq. (5), then defines a manifold in the (D_{xx}, D_{xy}) plane where there exist deformed polygons that satisfy the isoperimetric constraint [Fig. 5(a)]. The maximum value of D_{xy} along the isoperimetric contour defines the largest simple shear $D_{xy}^{\max}$ that a cell can sustain by changing its shape, while maintaining its area and perimeter constant. This value is $\gamma = \gamma_C = D_{xy}^{\max} \propto (p_0 - p_0^*)^{1/2}$ and precisely

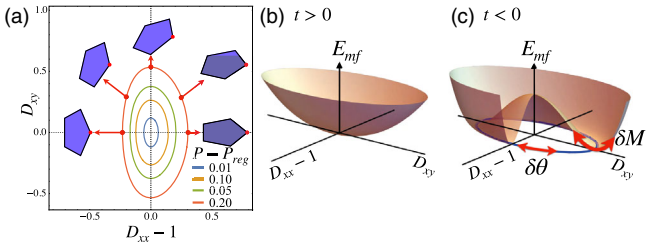

FIG. 5. (a) When the perimeter of a polygon is larger than that of its regular counterpart, deformations can lead to a family of isoperimetric shapes defined by the contours shown for a five-sided polygon. (b) The mean-field energy as a function of $(D_{xx} - 1, D_{xy})$ for $t > 0$ has a single ground state. (c) The mean-field energy as a function of $(D_{xx} - 1, D_{xy})$ for $t < 0$ has degenerate ground states that are connected by Goldstone modes along $\delta\theta$.

corresponds to the location of the strain-driven rigidity $\gamma = \gamma_C$ in the simulations. The exponent $1/2$ is in excellent agreement with the γ_C scaling in the vicinity of p_0^*, shown in the inset of Fig. 1.

The isoperimetric contours are centered at ($D_{xx} = 1$, $D_{xy} = 0$) and well approximated by an ellipse for small $P - P_{\mathrm{reg}}$. We introduce polar coordinates with radius $M(\theta)$ and polar angle θ: $D_{xx} - 1 = M(\theta)\cos\theta$ and $D_{xy} = M(\theta)\sin\theta$ and expand Eq. (5) to $\mathcal{O}(M^2)$ to give (see Supplemental Material [85])

$$P \approx P_{\mathrm{reg}} + \frac{15}{32} P_{\mathrm{reg}} \left[1 + \frac{3}{5}\cos(2\theta)\right] M(\theta)^2. \tag{6}$$

Using Eq. (6), we rewrite the vertex model energy [Eq. (1)] to obtain a Landau-type energy

$$E_{mf} = \frac{1}{2} t\alpha m(\theta, M)^2 + \frac{1}{4}\beta m(\theta, M)^4, \tag{7}$$

where $m(\theta, M) = [1 + (3/5)\cos(2\theta)]^{1/2} M$ is the order parameter, $\alpha = (60/32)p_0^{*2}, \beta = (30/32)p_0^{*2}$ are positive constants, and $t = (p_0^* - p_0)/p_0^*$ controls the distance to a continuous phase transition in $m(\theta, M)$. For $t > 0$, E_{mf} has a single minimum at $m^* = 0$ [Fig. 5(b)], corresponding to the rigid state. When $t < 0$, the minimum $m^*(\theta, M)$ corresponds to the isoperimetrically degenerate liquid state. In the energy landscape these states are connected by a Goldstone mode [Fig. 5(c)].

The MFT explains the origin of the nonlinear elasticity. For $t > 0$, E_{mf} has a single minimum at $m^* = 0$ (corresponding to an undeformed solid state) and deformations away from it can be calculated using Eq. (7)

$$\begin{aligned} \sigma &= \partial E_{mf}/\partial m = \alpha t m + \beta m^3, \\ G &= \partial^2 E_{mf}/\partial m^2 = \alpha t + 3\beta m^2. \end{aligned} \tag{8}$$

For small m we recover linear elasticity with $G_0 = \alpha t \propto (p_0^* - p_0)$. At large m the response is nonlinear, with $G \propto \sigma^{2/3}$. The crossover stress between the two regimes can be calculated: $\sigma_c = 2\beta\alpha^{3/2}t^{3/2} \propto (p_0^* - p_0)^{3/2}$. These predictions are in excellent agreement with simulation results.

We have used a vertex model to study the nonlinear response of a tissue to shear. Using simulations and MFT, we showed that a tissue that is liquid when unstrained stiffens upon shear. Liquid-solid transitions in VM of biological tissues are driven by geometric frustration and active mechanisms. Recent work by some of us [66] showed that geometric incompatibility controls the response to infinitesimal deformations, providing the underlying unifying mechanism for rigidity in a broad class of underconstrained systems. The present Letter additionally incorporates active processes that mediate plastic response. Plasticity dominates at higher strains and is likely to underlie the rheology of real tissue. Both works use a MFT to highlight the geometric origin of the degeneracy of the liquid ground state. The same MFT is extended here to investigate the response to deformations. While a Voronoi-based model is used, we have observed the same quantitative behavior using a vertex-based model and the results are independent of the model implementation.

Finally, it was shown in Ref. [66] that at the critical point the VM shares many of the properties of odd elasticity [101]—for instance, spontaneous shear upon uniaxial extension—although this behavior arises from geometry, not from an energy input at the microscale. Exploring the response to deformations other than simple shear and the possible connections with odd elasticity is an important direction for future work.

The authors thank Mark Bowick, Michael Moshe and Arthur Hernandez for illuminating discussions. This work was supported in part by the Northeastern University TIER 1 Grant (J. H. and D. B.), NSF DMR-2046683 (J. H. and D. B.), DMR-2041459 (M. C. M.), PHY-1748958 (D. B. and M. C. M.), the Center for Theoretical Biological Physics NSF PHY-2019745 (J. H. and D. B.) and MathWorks Microgrants. We acknowledge the support of the Northeastern University Discovery Cluster. This project has received funding from the European Research Council (ERC) under the European Union's Horizon 2020 research and innovation programme (Grant Agreement No. 885146); and the SOFI CDT, Durham University, EPSRC (EP/L015536/1).

[1] P. Kollmannsberger and B. Fabry, Linear and nonlinear rheology of living cells, Annu. Rev. Mater. Res. **41**, 75 (2011).
[2] J. Guck, R. Ananthakrishnan, H. Mahmood, T. J. Moon, C. C. Cunningham, and J. Käs, The optical stretcher: A novel laser tool to micromanipulate cells, Biophys. J. **81**, 767 (2001).
[3] K. Haase and A. E. Pelling, Investigating cell mechanics with atomic force microscopy, J. R. Soc. Interface **12**, 20140970 (2015).
[4] Y. Brill-Karniely, Mechanical measurements of cells using afm: 3d or 2d physics?, Front. Bioeng. Biotechnol. **8**, 1265 (2020).
[5] Y. Fujii, Y. Ochi, M. Tuchiya, M. Kajita, Y. Fujita, Y. Ishimoto, and T. Okajima, Spontaneous spatial correlation of elastic modulus in jammed epithelial monolayers observed by afm, Biophys. J. **116**, 1152 (2019).
[6] F. Serwane, A. Mongera, P. Rowghanian, D. A. Kealhofer, A. A. Lucio, Z. M. Hockenbery, and O. Campas, In vivo quantification of spatially varying mechanical properties in developing tissues, Nat. Methods **14**, 181 (2017).
[7] B. D. Hoffman, G. Massiera, K. M. Van Citters, and J. C. Crocker, The consensus mechanics of cultured mammalian cells, Proc. Natl. Acad. Sci. U.S.A. **103**, 10259 (2006).

[8] P. Fernández, P. A. Pullarkat, and A. Ott, A master relation defines the nonlinear viscoelasticity of single fibroblasts, Biophys. J. **90**, 3796 (2006).
[9] U. S. Schwarz and J. R. Soiné, Traction force microscopy on soft elastic substrates: A guide to recent computational advances, Biochim. Biophys. Acta **1853**, 3095 (2015).
[10] D. T. Tambe, U. Croutelle, X. Trepat, C. Y. Park, J. H. Kim, E. Millet, J. P. Butler, and J. J. Fredberg, Monolayer stress microscopy: Limitations, artifacts, and accuracy of recovered intercellular stresses, PLoS One **8**, e55172 (2013).
[11] J. P. Butler, I. M. Tolic-Nørrelykke, B. Fabry, and J. J. Fredberg, Traction fields, moments, and strain energy that cells exert on their surroundings, Am. J. Physiol. **282**, C595 (2002).
[12] A. F. Mertz, Y. Che, S. Banerjee, J. M. Goldstein, K. A. Rosowski, S. F. Revilla, C. M. Niessen, M. C. Marchetti, E. R. Dufresne, and V. Horsley, Cadherin-based intercellular adhesions organize epithelial cell–matrix traction forces, Proc. Natl. Acad. Sci. U.S.A. **110**, 842 (2013).
[13] A. F. Mertz, S. Banerjee, Y. Che, G. K. German, Y. Xu, C. Hyland, M. C. Marchetti, V. Horsley, and E. R. Dufresne, Scaling of traction forces with the size of cohesive cell colonies, Phys. Rev. Lett. **108**, 198101 (2012).
[14] X. Trepat, M. R. Wasserman, T. E. Angelini, E. Millet, D. A. Weitz, J. P. Butler, and J. J. Fredberg, Scaling of traction forces with the size of cohesive cell colonies, Nat. Phys. **5**, 426 (2009).
[15] J. H. Kim, X. Serra-Picamal, D. T. Tambe, E. H. Zhou, C. Y. Park, M. Sadati, J.-A. Park, R. Krishnan, B. Gweon, E. Millet *et al.*, Propulsion and navigation within the advancing monolayer sheet, Nat. Mater. **12**, 856 (2013).
[16] S. Getsios, A. C. Huen, and K. J. Green, Working out the strength and flexibility of desmosomes, Nat. Rev. Mol. Cell Biol. **5**, 271 (2004).
[17] N. Wang, J. D. Tytell, and D. E. Ingber, Mechanotransduction at a distance: mechanically coupling the extracellular matrix with the nucleus, Nat. Rev. Mol. Cell Biol. **10**, 75 (2009).
[18] F. Martino, A. R. Perestrelo, V. Vinarský, S. Pagliari, and G. Forte, Cellular mechanotransduction: From tension to function, Frontiers of oral physiology **9**, 824 (2018).
[19] H. Zhang and M. Labouesse, Signalling through mechanical inputs—a coordinated process, J. Cell Sci. **125**, 3039 (2012).
[20] T. Das, K. Safferling, S. Rausch, N. Grabe, H. Boehm, and J. P. Spatz, A molecular mechanotransduction pathway regulates collective migration of epithelial cells, Nat. Cell Biol. **17**, 276 (2015).
[21] P. Hayes and J. Solon, Drosophila dorsal closure: An orchestra of forces to zip shut the embryo, Mech. Dev. **144**, 2 (2017).
[22] P. F. Machado, J. Duque, J. Étienne, A. Martinez-Arias, G. B. Blanchard, and N. Gorfinkiel, Emergent material properties of developing epithelial tissues, BMC Biol. **13**, 98 (2015).
[23] D. J. Andrew and A. J. Ewald, Morphogenesis of epithelial tubes: Insights into tube formation, elongation, and elaboration, Dev. Biol. **341**, 34 (2010).
[24] R. Etournay, M. Popović, M. Merkel, A. Nandi, C. Blasse, B. Aigouy, H. Brandl, G. Myers, G. Salbreux, F. Jülicher, and S. Eaton, Interplay of cell dynamics and epithelial tension during morphogenesis of the *Drosophila* pupal wing, eLife **4**, e07090 (2015).
[25] B. Guirao, S. U. Rigaud, F. Bosveld, A. Bailles, J. López-Gay, S. Ishihara, K. Sugimura, F. Graner, and Y. Bellaïche, Unified quantitative characterization of epithelial tissue development, eLife **4**, e08519 (2015).
[26] T. Lecuit, P.-F. Lenne, and E. Munro, Force generation, transmission, and integration during cell and tissue morphogenesis, Annu. Rev. Cell Dev. Biol. **27**, 157 (2011).
[27] R. J. Tetley, M. F. Staddon, D. Heller, A. Hoppe, S. Banerjee, and Y. Mao, Tissue fluidity promotes epithelial wound healing, Nat. Phys. **15**, 1 (2019).
[28] X. Wang, M. Merkel, L. B. Sutter, G. Erdemci-Tandogan, M. L. Manning, and K. E. Kasza, Anisotropy links cell shapes to tissue flow during convergent extension, Proc. Natl. Acad. Sci. U.S.A. **117**, 13541 (2020).
[29] A. B. Fisher, S. Chien, A. I. Barakat, and R. M. Nerem, Endothelial cellular response to altered shear stress, Am. J. Physiol.**281**, L529 (2001).
[30] X. Trepat, L. Deng, S. S. An, D. Navajas, D. J. Tschumperlin, W. T. Gerthoffer, J. P. Butler, and J. J. Fredberg, Universal physical responses to stretch in the living cell, Nature (London) **447**, 592 (2007).
[31] J. Comelles, S. SS, L. Lu, E. Le Maout, S. Anvitha, G. Salbreux, F. Jülicher, M. M. Inamdar, and D. Riveline, Epithelial colonies in vitro elongate through collective effects, eLife **10**, e57730 (2021).
[32] D. T. Tambe, C. C. Hardin, T. E. Angelini, K. Rajendran, C. Y. Park, X. Serra-Picamal, E. H. Zhou, M. H. Zaman, J. P. Butler, D. A. Weitz *et al.*, Collective cell guidance by cooperative intercellular forces, Nat. Mater. **10**, 469 (2011).
[33] M. Vishwakarma, J. Di Russo, D. Probst, U. S. Schwarz, T. Das, and J. P. Spatz, Mechanical interactions among followers determine the emergence of leaders in migrating epithelial cell collectives, Nat. Commun. **9**, 3469 (2018).
[34] D. T. Butcher, T. Alliston, and V. M. Weaver, A tense situation: forcing tumour progression, Nat. Rev. Cancer **9**, 108 (2009).
[35] D. Wirtz, K. Konstantopoulos, and P. C. Searson, The physics of cancer: the role of physical interactions and mechanical forces in metastasis, Nat. Rev. Cancer **11**, 512 (2011).
[36] R. K. Jain, J. D. Martin, and T. Stylianopoulos, The role of mechanical forces in tumor growth and therapy, Annu. Rev. Biomed. Eng. **16**, 321 (2014).
[37] A. R. Harris, L. Peter, J. Bellis, B. Baum, A. J. Kabla, and G. T. Charras, Characterizing the mechanics of cultured cell monolayers, Proc. Natl. Acad. Sci. U.S.A. **109**, 16449 (2012).
[38] N. Khalilgharibi, J. Fouchard, N. Asadipour, R. Barrientos, M. Duda, A. Bonfanti, A. Yonis, A. Harris, P. Mosaffa, Y. Fujita *et al.*, Stress relaxation in epithelial monolayers is controlled by the actomyosin cortex, Nat. Phys. **15**, 839 (2019).
[39] E. Sadeghipour, M. A. Garcia, W. J. Nelson, and B. L. Pruitt, Shear-induced damped oscillations in an epithelium depend on actomyosin contraction and e-cadherin cell adhesion, eLife **7**, e39640 (2018).

[40] V. N. Prakash, M. S. Bull, and M. Prakash, Motility-induced fracture reveals a ductile-to-brittle crossover in a simple animal's epithelia, Nat. Phys. **17**, 504 (2021).
[41] E. Latorre, S. Kale, L. Casares, M. Gómez-González, M. Uroz, L. Valon, R. V. Nair, E. Garreta, N. Montserrat, A. Del Campo *et al.*, Active superelasticity in three-dimensional epithelia of controlled shape, Nature (London) **563**, 203 (2018).
[42] J.-A. Park *et al.*, Unjamming and cell shape in the asthmatic airway epithelium, Nat. Mater. **14**, 1040 (2015).
[43] S. Garcia, E. Hannezo, J. Elgeti, J.-F. Joanny, P. Silberzan, and N. S. Gov, Physics of active jamming during collective cellular motion in a monolayer, Proc. Natl. Acad. Sci. U.S.A. **112**, 15314 (2015).
[44] L. Oswald, S. Grosser, D. M. Smith, and J. A. Käs, Jamming transitions in cancer, J. Phys. D **50**, 483001 (2017).
[45] C. D. Paul, P. Mistriotis, and K. Konstantopoulos, Cancer cell motility: Lessons from migration in confined spaces, Nat. Rev. Cancer **17**, 131 (2017).
[46] C. Malinverno, S. Corallino, F. Giavazzi, M. Bergert, Q. Li, M. Leoni, A. Disanza, E. Frittoli, A. Oldani, E. Martini *et al.*, Endocytic reawakening of motility in jammed epithelia, Nat. Mater. **16**, 587 (2017).
[47] L. Atia, D. Bi, Y. Sharma, J. A. Mitchel, B. Gweon, S. A. Koehler, S. J. DeCamp, B. Lan, J. H. Kim, R. Hirsch *et al.*, Geometric constraints during epithelial jamming, Nat. Phys. **14**, 613 (2018).
[48] A. Mongera, P. Rowghanian, H. J. Gustafson, E. Shelton, D. A. Kealhofer, E. K. Carn, F. Serwane, A. A. Lucio, J. Giammona, and O. Campàs, A fluid-to-solid jamming transition underlies vertebrate body axis elongation, Nature (London) **561**, 401 (2018).
[49] O. Ilina, P. G. Gritsenko, S. Syga, J. Lippoldt, C. A. M. La Porta, O. Chepizhko, S. Grosser, M. Vullings, G.-J. Bakker, J. Starruß, P. Bult, S. Zapperi, J. A. Käs, A. Deutsch, and P. Friedl, Cell–cell adhesion and 3d matrix confinement determine jamming transitions in breast cancer invasion, Nat. Cell Biol. **22**, 1103 (2020).
[50] R. J. Huebner, A. N. Malmi-Kakkada, S. Sarikaya, S. Weng, D. Thirumalai, and J. B. Wallingford, Cadherin clustering controls heterogeneous, asymmetric junction dynamics during vertebrate axis elongation, bioRxiv 10.1101/2020.02.11.944033 (2020).
[51] J. A. Mitchel, A. Das, M. J. O'Sullivan, I. T. Stancil, S. J. DeCamp, S. Koehler, O. H. Ocaña, J. P. Butler, J. J. Fredberg, M. A. Nieto *et al.*, In primary airway epithelial cells, the unjamming transition is distinct from the epithelial-to-mesenchymal transition, Nat. Commun. **11**, 1 (2020).
[52] N. I. Petridou, B. Corominas-Murtra, C.-P. Heisenberg, and E. Hannezo, Rigidity percolation uncovers a structural basis for embryonic tissue phase transitions, Cell **184**, 1914 (2021).
[53] S.-Z. Lin, W.-Y. Zhang, D. Bi, B. Li, and X.-Q. Feng, Energetics of mesoscale cell turbulence in two-dimensional monolayers, Commun. Phys. **4**, 21 (2021).
[54] H. Yang, A. F. Pegoraro, Y. Han, W. Tang, R. Abeyaratne, D. Bi, and M. Guo, Configurational fingerprints of multicellular living systems, Proc. Natl. Acad. Sci. U.S.A. **118**, e2109168118 (2021).
[55] M. D. Marzio, A. Kılıç, E. Maiorino, J. A. Mitchel, C. Mwase, M. J. O'Sullivan, M. McGill, R. Chase, J. J. Fredberg, J.-A. Park, K. Glass, and S. T. Weiss, Genomic signatures of the unjamming transition in compressed human bronchial epithelial cells, Sci. Adv. **7**, eabf1088 (2021).
[56] T. Nagai and H. Honda, A dynamic cell model for the formation of epithelial tissues, Philos. Mag. B **81**, 699 (2001).
[57] R. Farhadifar, J.-C. Röper, B. Aigouy, S. Eaton, and F. Jülicher, The influence of cell mechanics, cell-cell interactions, and proliferation on epithelial packing, Curr. Biol. **17**, 2095 (2007).
[58] S. Tong, N. K. Singh, R. Sknepnek, and A. Kosmrlj, Linear viscoelastic properties of the vertex model for epithelial tissues, arXiv:2102.11181.
[59] M. Popović, V. Druelle, N. A. Dye, F. Jülicher, and M. Wyart, Inferring the flow properties of epithelial tissues from their geometry, New J. Phys. **23**, 033004 (2021).
[60] C. Duclut, J. Paijmans, M. M. Inamdar, C. D. Modes, and F. Jülicher, Nonlinear rheology of cellular networks, Cells Dev. 203746 (2021).10.1016/j.cdev.2021.203746
[61] A. Pasupalak, S. K. Samidurai, Y. Li, Y. Zheng, R. Ni, and M. P. Ciamarra, Unconventional rheological properties in systems of deformable particles, Soft Matter **17**, 7708 (2021).
[62] M. Krajnc, T. Stern, and C. Zankoc, Active Instability and Nonlinear Dynamics of Cell-Cell Junctions, Phys. Rev. Lett. **127**, 198103 (2021).
[63] G.-K. Xu, Y. Liu, and B. Li, How do changes at the cell level affect the mechanical properties of epithelial monolayers?, Soft Matter **11**, 8782 (2015).
[64] A. Merzouki, O. Malaspinas, and B. Chopard, The mechanical properties of a cell-based numerical model of epithelium, Soft Matter **12**, 4745 (2016).
[65] D. Bi, J. Zhang, B. Chakraborty, and R. P. Behringer, Jamming by shear, Nature (London) **480**, 355 (2011).
[66] A. Hernandez, M. F. Staddon, M. J. Bowick, M. C. Marchetti, and M. Moshe, Geometric rigidity and anomalous elasticity of cellular tissue vertex model, arXiv:2109.10407.
[67] D. Bi, X. Yang, M. C. Marchetti, and M. L. Manning, Motility-Driven Glass and Jamming Transitions in Biological Tissues, Phys. Rev. X **6**, 021011 (2016).
[68] B. Li and S. X. Sun, Coherent motions in confluent cell monolayer sheets, Biophys. J. **107**, 1532 (2014).
[69] X. Li, A. Das, and D. Bi, Mechanical Heterogeneity in Tissues Promotes Rigidity and Controls Cellular Invasion, Phys. Rev. Lett. **123**, 058101 (2019).
[70] X. Li, A. Das, and D. Bi, Biological tissue-inspired tunable photonic fluid, Proc. Natl. Acad. Sci. U.S.A. **115**, 6650 (2018).
[71] L. Yan and D. Bi, Multicellular Rosettes Drive Fluid-Solid Transition in Epithelial Tissues, Phys. Rev. X **9**, 011029 (2019).
[72] A. Das, S. Sastry, and D. Bi, Controlled Neighbor Exchanges Drive Glassy Behavior, Intermittency, and Cell Streaming in Epithelial Tissues, Phys. Rev. X **11**, 041037 (2021).
[73] D. B. Staple, R. Farhadifar, J. C. Röper, B. Aigouy, S. Eaton, and F. Jülicher, Mechanics and remodelling of cell packings in epithelia, Eur. Phys. J. E **33**, 117 (2010).

[74] D. Bi, J. H. Lopez, J. M. Schwarz, and M. L. Manning, A density-independent rigidity transition in biological tissues, Nat. Phys. **11**, 1074 (2015).
[75] M. P. Allen and D. J. Tildesley, *Computer Simulation of Liquids* (Clarendon Press, New York, NY, USA, 1989).
[76] E. Bitzek, P. Koskinen, F. Gähler, M. Moseler, and P. Gumbsch, Structural Relaxation Made Simple, Phys. Rev. Lett. **97**, 170201 (2006).
[77] D. M. Sussman and M. Merkel, No unjamming transition in a voronoi model of biological tissue, Soft Matter **14**, 3397 (2018).
[78] O. K. Damavandi, V. F. Hagh, C. D. Santangelo, and M. L. Manning, Energetic rigidity. i. a unifying theory of mechanical stability, Phys. Rev. E **105**, 025003 (2022).
[79] M. Moshe, M. J. Bowick, and M. C. Marchetti, Geometric Frustration and Solid-Solid Transitions in Model 2d Tissue, Phys. Rev. Lett. **120**, 268105 (2018).
[80] M. Merkel, K. Baumgarten, B. P. Tighe, and M. L. Manning, A minimal-length approach unifies rigidity in underconstrained materials, Proc. Natl. Acad. Sci. U.S.A. **116**, 6560 (2019).
[81] R. Kupferman, B. Maman, and M. Moshe, Continuum mechanics of a cellular tissue model, J. Mech. Phys. Solids **143**, 104085 (2020).
[82] S. Ishihara and K. Sugimura, Bayesian inference of force dynamics during morphogenesis, J. Theor. Biol. **313**, 201 (2012).
[83] K. K. Chiou, L. Hufnagel, and B. I. Shraiman, Mechanical stress inference for two dimensional cell arrays, PLoS Comput. Biol. **8**, e1002512 (2012).
[84] X. Yang, D. Bi, M. Czajkowski, M. Merkel, M. L. Manning, and M. C. Marchetti, Correlating cell shape and cellular stress in motile confluent tissues, Proc. Natl. Acad. Sci. U.S.A. **114**, 12663 (2017).
[85] See Supplemental Material at http://link.aps.org/supplemental/10.1103/PhysRevLett.128.178001, which contains additional details on the model, additional results complementing those shown in the main text, and includes Refs. [86–92].
[86] M. Czajkowski, D. Bi, M. L. Manning, and M. C. Marchetti, Hydrodynamics of shape-driven rigidity transitions in motile tissues, Soft Matter **14**, 5628 (2018).
[87] M. Aubouy, Y. Jiang, J. A. Glazier, and F. Graner, A texture tensor to quantify deformations, Granular Matter **5**, 67 (2003).
[88] B. Aigouy, R. Farhadifar, D. B. Staple, A. Sagner, J.-C. Röper, F. Jülicher, and S. Eaton, Cell Flow Reorients the Axis of Planar Polarity in the Wing Epithelium of Drosophila, Cell **142**, 773 (2010).
[89] F. Graner, B. Dollet, C. Raufaste, and P. Marmottant, Discrete rearranging disordered patterns, part I: Robust statistical tools in two or three dimensions, Eur. Phys. J. E **25**, 349 (2008).
[90] M. Rauzi, P. Verant, T. Lecuit, and P.-F. Lenne, Nature and anisotropy of cortical forces orienting drosophila tissue morphogenesis, Nat. Cell Biol. **10**, 1401 (2008).
[91] F. Bosveld, I. Bonnet, B. Guirao, S. Tlili, Z. Wang, A. Petitalot, R. Marchand, P.-L. Bardet, P. Marcq, F. Graner, and Y. Bellaiche, Mechanical control of morphogenesis by fat/dachsous/four-jointed planar cell polarity pathway, Science **336**, 724 (2012).
[92] T. H. Courtney, *Mechanical Behavior of Materials* (Waveland Press, Long Grove, Illinois, 2005).
[93] K. VanderWerf, A. Boromand, M. D. Shattuck, and C. S. O'Hern, Pressure Dependent Shear Response of Jammed Packings of Frictionless Spherical Particles, Phys. Rev. Lett. **124**, 038004 (2020).
[94] S. A. Langer and A. J. Liu, Effect of random packing on stress relaxation in foam, J. Phys. Chem. B **101**, 8667 (1997).
[95] B. A. DiDonna and T. C. Lubensky, Nonaffine correlations in random elastic media, Phys. Rev. E **72**, 066619 (2005).
[96] C. P. Broedersz and F. C. MacKintosh, Modeling semiflexible polymer networks, Rev. Mod. Phys. **86**, 995 (2014).
[97] M. E. Gurtin, E. Fried, and L. Anand, *The Mechanics and Thermodynamics of Continua* (Cambridge University Press, Cambridge, England, 2010).
[98] J. D. Goddard, Continuum modeling of granular assemblies, in *Physics of Dry Granular Media*, edited by H. J. Herrmann, J.-P. Hovi, and S. Luding (Springer Netherlands, Dordrecht, 1998), pp. 1–24.
[99] P. K. Singh, J. C.-W. Lee, K. A. Patankar, and S. A. Rogers, Revisiting the basis of transient rheological material functions: Insights from recoverable strain measurements, J. Rheol. **65**, 129 (2021).
[100] A. Hernandez and M. C. Marchetti, Poisson-bracket formulation of the dynamics of fluids of deformable particles, Phys. Rev. E **103**, 032612 (2021).
[101] C. Scheibner, A. Souslov, D. Banerjee, P. Surówka, W. T. Irvine, and V. Vitelli, Odd elasticity, Nat. Phys. **16**, 475 (2020).